We are IntechOpen, the world's leading publisher of Open Access books Built by scientists, for scientists

6,900
Open access books available

185,000
International authors and editors

200M
Downloads

Our authors are among the

154
Countries delivered to

TOP 1%
most cited scientists

12.2%
Contributors from top 500 universities



WEB OF SCIENCE™

Selection of our books indexed in the Book Citation Index in Web of Science™ Core Collection (BKCI)

Interested in publishing with us?
Contact book.department@intechopen.com

Numbers displayed above are based on latest data collected.
For more information visit www.intechopen.com



12

Integrated Microfluidic MEMS and Their Biomedical Applications

Abdulilah A. Dawoud Bani-Yaseen
Department of Chemistry, Faculty of Science Taibah University, Al-Madinah Al-Munawarah P.O. Box 30002, KSA

1. Introduction

Microfluidic technology has been revolutionizing the landscape of various fields of analytical sciences since its introduction back in the early 1990s [1,2]. This emerging technology offers a variety of advantages over conventional pinch-top chemical instrumentation, such as performing rapid and low cost analysis, integrating various functional elements onto a single platform, consuming minimal amount of reagents and hence producing nominal waste volumes, and being more amenable for portability and automation. Interestingly, such superiority of these advantages has been demonstrated via utilizing various microfluidic systems in performing a wide range of tasks for various applications; this includes biomedical diagnostics [3-6], genomic and proteomics analyses [7-11], drug discovery and delivery [12-14], and environmental investigations [15-18]. On the other hand, integrated microfluidic systems has recently gained a great amount of attention, where the operation process of the microfluidic system is fully controlled via integrated circuit, which in systems defined as microfluidic micro-electro-mechanical-systems (MEMS), i.e. microfluidic MEMS.

While the microfluidic technology can be utilized to perform different functionalities, microfluidic devices that function based on the phenomenon of capillary-electrophoresis (CE) still the main applicability of this technology [2, 19-22]. Practically, the CE-based microfluidic devices are utilized to perform sample injection, separation, and detection of a wide range of analytes. Recently, there has been a great interest in integrating various detection modes, such as electrochemical and optical detectors, onto microfluidic devices of various architectures and designs [23-26]. However, notable attentions toward electrochemical detection (ECD), amperometric detection in particular, have increased. Although laser induced fluorescence (LIF) is considered as the most sensitive detection mode interfaced with various separation methods including the microfluidic technology, LIF is ineffective in detecting molecules that exhibit weak native fluorescence at room temperature, such as DNA adducts. Thus, ECD, amperometry in particular, offers an effective remedy for detecting those molecules that are natively weak fluorescent at room temperature such as Dopamine (DA)-derived DNA adduct (4DA-6-N7Gua) and 8-Hydroxy-2′-deoxyguanosine (8-OH-dG) adduct [26, 27].

Interfacing integrated ECD with CE-based microfluidic devices can fully exploit many advantages of miniaturization. The sensing electrodes can be arranged in two distinctive arrangements, namely in-channel and end-channel detection. However, the influence of the

electrophoretic current on the detection current necessitates the introduction of a decoupler for the in-channel detection, whereas optimizing the location of the sensing electrodes near the exit of the separation channel is necessary for end-channel detection. We have shown that introducing a palladium decoupler for in-channel ECD significantly enhanced the stability of the sensing electrode, where the limit of detection (LOD) for sensing 8-OH-dG was lowered one order of magnitude for the in-channel ECD in comparison to the end-channel ECD that was used for sensing 4DA-6-N7Gua [27]. The palladium decoupler was introduced implementing the electroplating technique for depositing nano size palladium particles on the surface of integrated gold microelectrodes. On the other hand, we have reported implementing the electroplating technique for enhancing the coulometric efficiency (C_{eff}) of an integrated gold microelectrode for sensing selected biotargets, such as DA, where C_{eff} was tripled for roughened electroplated sensing gold electrode in comparison to bare electrodes [28].

DNA adducts formation that results from covalent interaction of genotoxic carcinogens with DNA can create various mutations in some critical genes and subsequently development of various diseases, such as cancer [29,30]. There are two general pathways for the formation of the DNA adducts; first, direct binding of some genotoxic carcinogens DNA to create the mutation, the second pathway proceeds via certain metabolic pathways, where some active metabolites can react with the DNA to form the adducts [31,32]. The role of DNA damage and subsequently formation of DNA adducts that can be considered as potential biomarkers are of particular importance in studies involving cancer and other diseases [33-36]. In this chapter, the fabrication and applicability of microfluidic devices with integrated ECD for the analysis of DNA adducts, namely 4DA-6-N7Gua and 8-OH-dG adducts are outlined. In particular, the applicability of the microfluidic device with end-channel and in-channel detections was evaluated for the analysis of 4DA-6-N7Gua and 8-OH-dG DNA adducts, respectively.

2. Principle of operation

In CE-based microfluidic systems, the flow of liquids inside the microchannels is driven according to the electrokinetic phenomenon. On the other hand, electrophoresis is defined as the migration of electrically charged specie under the influence of external electric field. As many details pertaining to this phenomenon can be found in the literature, brief description of this phenomenon is provided here. Wide range of solid materials acquires surface charge upon coming into contact with electrolytes, where this surface charge attracts counter charged species to form a very thin layer, which in turn known as Stern layer and consequently another layer is formed under the influence of Stern layer known as Gouy-Chapman layer. Hence, both layers jointly form the electrical double layer (EDL). It is noteworthy mentioning that the formation of EDL is mandatory to generate a flow inside the microchannels, where upon applying an electric field along the microchannel; charged species as well as solvent molecules migrate toward the counter charged electrodes to generate what is known as the electroosmotic flow (EOF). The speed of EOF (u_{EOF}) is governed according to Helmholtz-Smoluchowski equation [37,38]:

$$u_{EOF} = \frac{\varepsilon E_{el} \xi}{\eta} \tag{1}$$

where, ε is the dielectric constant, η is viscosity of the solution, E_{el} is strength of the electric field, ξ is the zeta potential.
However, as the u_{EOF} concerns the speed of bulk solution, mainly generated by migration of solvent molecules, another parameter that is characteristic for other charged species known as the electro-osmotic mobility (μ_e):

$$\mu_e \frac{q}{6\pi r\eta} \tag{2}$$

where, q is the ion charge, r is the ion radius. Furthermore, it is worth mentioning that CE is one type of electrophoresis with various modes, including Capillary Zone Electrophoresis (CZE), Capillary Isoelectric Focusing (CIEF), Capillary Gel Electrophoresis (CGE), Capillary Isotachophoresis (ITP), Capillary Electrokinetic Chromatography (EKC), Non-Aqueous Capillary Electrophoresis (NACE), and Capillary Electrochromatography (CEC). Hence, the common characteristic of all these modes of CE is the fact that they are electrophoretic processes performed in a capillary tube with usually a diameter that less than 100 μm. Thus, in caparison to the hydrodynamic driven flow inside the same capillary, one can notice that EOF and hydrodynamic driven flow profile flat and laminar flow with broad profile, respectively. Such observation can be attributed to the fact that there is no pressure drop along the capillary operating under EOF due to uniformity of EOF along the capillary, and hence flat profile is observed for the EOF. In addition, CE systems are used frequently for performing separation experiments that is analogous to other separation techniques, such as high performance liquid chromatography (HPLC), where the main task is to separate a mixture of various analytes into its components followed by analyzing these components quantitatively and/or qualitatively. It is noteworthy mentioning that all analytes migrate toward the cathode where a detector is aligned across the end of the capillary regardless their charge, and hence the migration of each analyte is characterized by the apparent electro-osmotic mobility (μ_a) instead of (μ_e), where (μ_a) and (μ_e) are correlated as:

$$\mu_a = \mu_e + \mu_{EOF} \tag{3}$$

On the other hand, various modes of detection have been interfaced with CE systems; this includes electrochemical detection (mainly amperometric and conductometric), laser induced fluorescence (LIF), UV-Vis absorption, Raman spectroscopy, mass spectrometry, H^1-NMR spectroscopy, refractive index spectroscopy, and FT-IR spectroscopy. In principle, all theories and mechanism of flow that govern CE systems can be extended to govern microfluidic systems operating under electrokinetic phenomenon. Commonly, a capillary that is made of silica is used for performing CE, where the double layer is constructed between the ionized hydroxyl groups ($Si\text{-}O^-$) and protons (H^+) that correspond to both surface charge and buffer species, respectively. Thus, it is essential to fabricate the microfluidic system from a material that can support the formation of the EDL. Hence, various types of materials have been utilized for fabricating microfluidic devices operating under electrokinetic phenomenon. Among these materials, glass and polymeric materials are the most popular ones. Glass exhibit characteristics, such has optically transparent, well-understood surface characteristics that are analogous to fused silica, chemicals resistant, and electrically insulator. On the other hand various types of polymers have been recently utilized for fabricating microfluidic systems; where among these materials PDMS is considered as the most popular one. However, while glass exhibit physicochemical

properties that are more analogous to fused silica than PDMS, its relatively more complicated fabrication procedure in comparison to PDMS renders its application in advanced microfluidic systems, such as integrated microfluidic MEMS. Furthermore, fabricating integrated necessitates the inclusion of detection mode to the microfluidic MEMS. Hence, integrating ECD to the microfluidic MEMS is considered the most practical approach in term ease and expenses of fabrication, which in turn if particular importance when disposability of biomedical Microdevices is needed. Figure 1 exhibits a schematic representation for CE interfaced with amperometric detection mode. As can be noticed, chemical specie in a reduced form migrates with the EOF at μ_a in the direction toward the electrophoretic cathode, where it is oxidized upon coming into contact with surface of the working electrode (WE) to generate a current that is proportional to its concentration. It is noteworthy mentioning herein that similar principle of operation is applied for microfluidic MEMS with EC detection presented in this chapter.

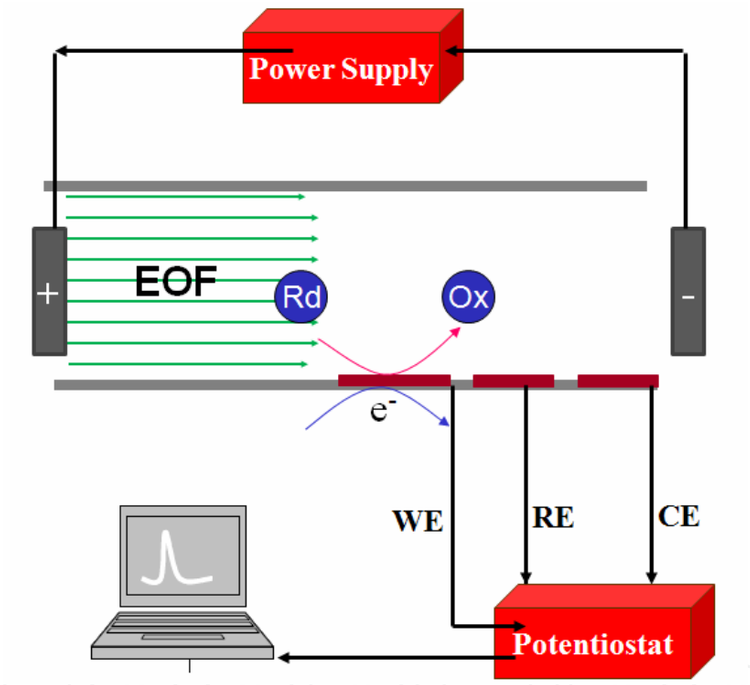


Fig. 1. Experimental setup for CE system interfaced with 3-electrode electrochemical configuration.

3. Experimental

3.1 Chemicals, reagents & materials:

DNA adducts: DA-derived DNA adduct (4DA-6-N7Gua), 2.8-Hydroxy-2'-deoxyguanosine (8-OHdG; neurotransmitters: dopamine, L-tyrosine, L-DOPA; separation buffers (10 mM): boric acid, monosodium phosphate, 2-[N-morpholino] ethanesulfonic acid (MES); Metals: gold, titanium; sodium hydroxide,), deoxyguanosine (dG), catechol; photoresists (SU-8 25, AZ-5214); photoresists developers (Microchem); gold etchant: iodine and potassium iodine (1:4, w:w); organic solvents: acetone, methanol, ethanol; Poly dimethylsiloxane (PDMS) (Sylgard 184); potassium hexachloropalladate (IV) (K_2PdCl_6); sodium tetrachloroaurate (III).

$2H_2O$ ($NaAuCl_4$. $2H_2O$); potassium hexachloroplatinate (IV) (K_2PtCl_6); morphine; codeine; glass microscopic slides; silicon wafers; and photomasks. All materials were purchased from commercial suppliers and were used as received, except for 4DA-6-N7Gua.

3.2 Equipments

Radio frequency (RF) plasma cleaner, resistive evaporation system, spin coater, stream of high purity nitrogen, UV light exposing system, potentiostat, DC power supply, picoammeter.

3.3 Methods

3.3.1 DNA adducts synthesis

Detailed outline for the synthesis of 4DA-6-N7Gua was published previously [39]; in brief:

1. DA is oxidized using silver oxide (Ag_2O) in dry dimethylformamide (DMF) to form the DA quinone.
2. The of solution of DA quinone is filtered onto a solution of dG in $CH_3COOH/DMF/H_2O$ (v:v:v, 1:1:1); the solution is stirred for approximately 10 hr at room temperature.
3. The 4DA-6-N7Gua adduct is purified using preparative HPLC system and can be verified using ^1H NMR and mass spectrometry.

3.3.2 Sample preparation

1. Stock solutions of 1mM of each analytes is prepared in the running buffer and kept frozen at -20 ˚C until further needed.
2. Analytes' solution with different desired concentrations can be prepared daily by diluting the stock solutions using the running buffer.
3. Various running buffers with a concentration of 10 mM and different pH were prepared by dissolving a desired amount of the buffer sample in highly pure water; adjustment to the desired pH was performed using a solution of 0.5 M NaOH.

3.3.3 Microfluidic devic1 Fabrication

3.3.3.1 PDMS microchannel fabrication

1. The PDMS slabs with microchannels network is prepared implementing the micromolding technique and using a mold that is made of SU-8025 photoresist polymerized on silicon wafer.
2. The mold is prepared by spin coating the photoresist on the surface of the silicon wafer, followed by the necessary drying process.
3. The desired architecture of the microchannels network is transferred onto the mold through exposing the silicon wafer (covered with the photoresist) to UV light through in-house prepared photomask, followed by the curing process.
4. Pre-polymerized PDMS solution is prepared and degassed shortly before starting the micromolding procedure.
5. The PDMS solution is poured onto the mold, followed by a curing process at 65˚C for 2 hr.
6. Then the PDMS slab is peeled off the mold gently and kept in clean area until further needed. Optimal microchannels' dimensions that are recommended are 25 and 75 μm for the depth and width, respectively. The length of the separation channel may vary, which depends on the resolution that is expected from the separation process; hence, longer separation channel is needed for better resolution.

3.3.3.2 Metalic microelectrodes fabrication

1. Pre-cleaned glass substrates are loaded inside the resistive evaporation chamber.
2. Two layers of titanium and gold are deposited onto the substrates surfaces with thickness of 10 and 200 nm, respectively.
3. Thin layer of photoresist (AZ-5214) is spun coated on the surface of the substrates then dried at 90˚C for 20 min.
4. The pattern of the microelectrodes is transferred to the substrates through exposing the substrates to UV light through a photomask that encloses the structure of the microelectrodes.
5. After the UV exposure, the photoresist is developed, followed by hardening process at 120˚C for 20 min.
6. The substrates are immersed inside freshly prepared solution of gold etchant with shaking for approximately 2 minutes.
7. After the etching process, the pattern of the microelectrodes is clear and the remaining photoresist is wiped away through rinsing the substrates with acetone then methanol in order to expose the surface of the gold electrodes.

3.3.3.3 Carbon microelectrodes fabrication

Schematic representation of the fabrication process is presented in Figure 2.

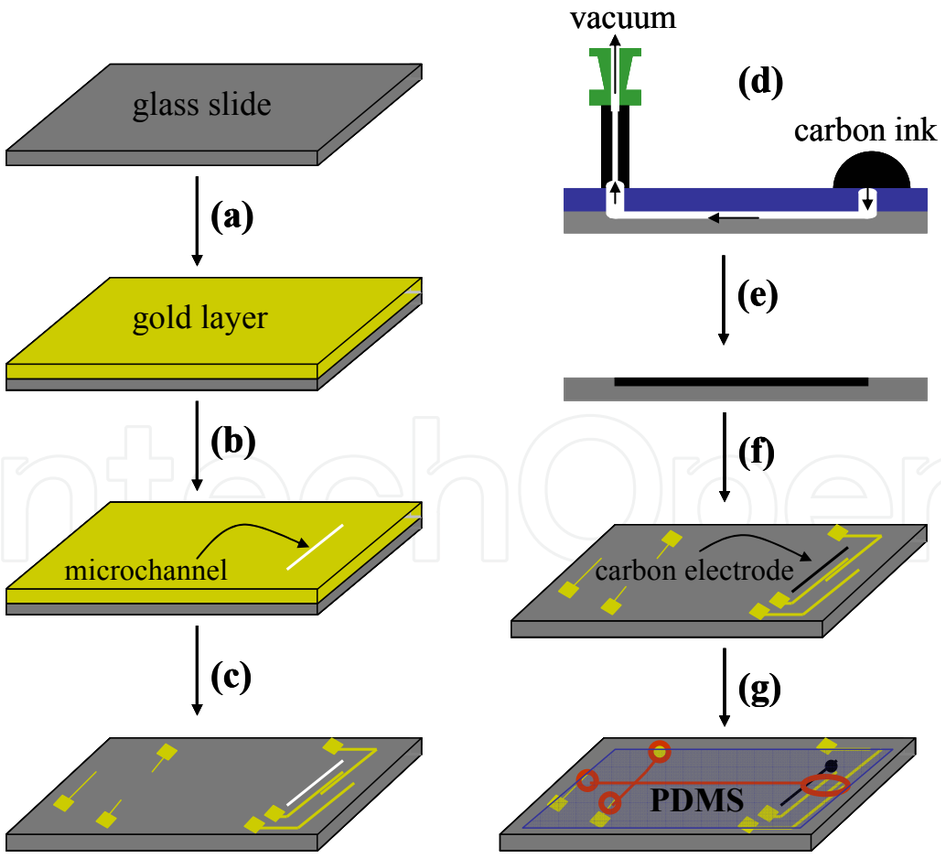


Fig. 2. Step-by-step procedure for microfabrication of carbon microelectrode integrated within microfluidic MEMS

1. Ending with the substrate in the previous section, thin layer of photoresist (AZ-5214) is spun coated on the surface of the substrates then dried at 90˚C for 20 min.
2. The pattern of the microchannel, where the carbon ink will be injected, is transferred to the substrates through exposing the substrates to UV light through a photomask that encloses the structure of the microchannel.
3. After the UV exposure, the photoresist is developed, followed by hardening process at 120˚C for 20 min.
4. Drops of buffered HF are added over the exposed area that defines the location of the microchannel on the substrate. The depth of the microchannel can measured frequently till reach an optimum depth of approximately 15 μm.
5. After the etching process, the pattern of the microelectrodes is clear and the remaining photoresist is wiped away through rinsing the substrates with acetone then methanol in order to expose the surface of the substrate.
6. Small piece of PDMS with two holes is bonded reversibly to the microelectrodes substrate, where the two holes on the PDMS match the two end of the microchannel.
7. A drop of the carbon ink is loaded into one hole while applying vacuum to the other hole.
8. The carbon ink will fill the microchannel, then the PDMS slab can be removed, and the carbon microelectrode is left for dryness at room temperature for 1 hr.

3.3.3.4 Microdevice assembling

9. The PDMS slab with the microchannels is cut onto the desired size using a lazar blade.
10. Four holes are created at the end of each microchannel using hand-punch holes maker.
11. For cleaning, the PDMS slab is immersed in ethanol and sonicated for 10 min., then dried at 60˚C.
12. Assembling the microfluidic device is carried out either reversibly or irreversibly by binding the PDMS slab with the microchannels to the gold-patterned glass substrate.

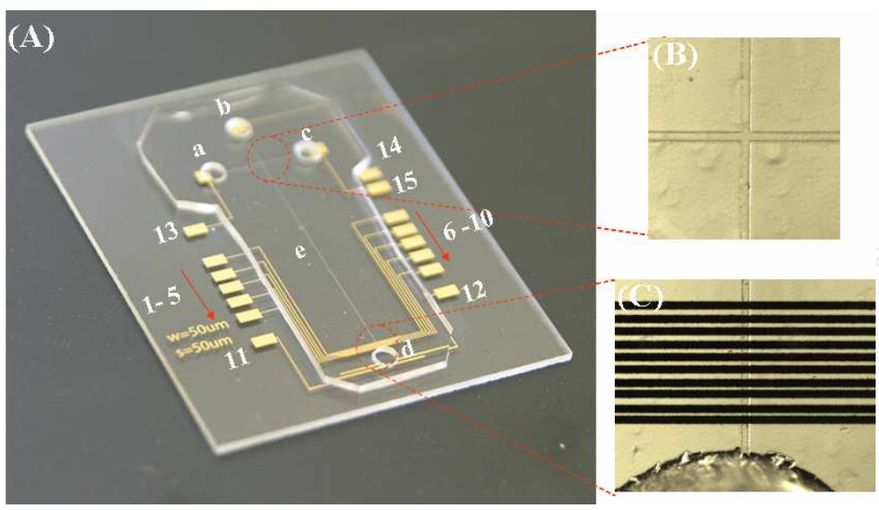


Fig. 3. Integrated microfluidic device with ECD (A): buffer reservoir (a), sample reservoir (b), waste reservoirs (c, d), separation channel (e), an array of working electrodes (1-10), reference electrode (11), auxiliary electrode (12), electrodes for injection and separation (13-15), frame (B): enlarged image for the microchannel where injection is performed; frame (C): enlarged image for the detection zone where the array of the microelectrodes are located. Note: the first electrode serves as decoupler for the in-channel detection.

13. To carry out the reversible binding, the PDMS slab is bound to the glass substrate without any further treatment.
14. For the irreversible binding, the PDMS slab and the glass substrate are subjected to RF-plasma treatment operating with stream of oxygen at 1-Torr for 1 min; then they are brought onto contact tightly. Figure 3 shows detailed image for the integrate microfluidic MEMS.

3.3.4 Electroplating procedure

Schematic representation for experimental setup of electrochemical deposition of metals nanoparticles son the surface of microelectrodes inside microchannels is presented in Figure 4.

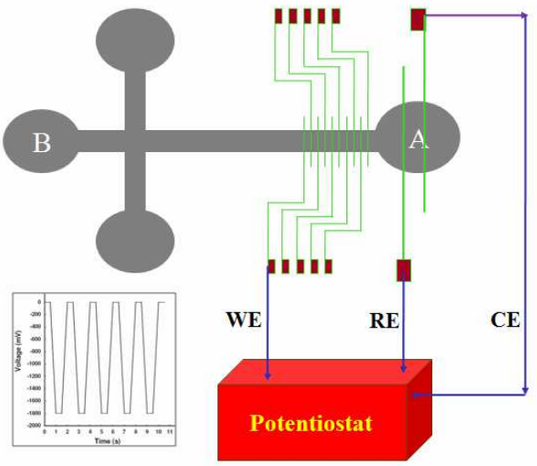


Fig. 4. Experimental setup for electrochemical deposition of metals nanoparticles on the surface of microelectrodes inside a microchannel of microfluidic MEMS

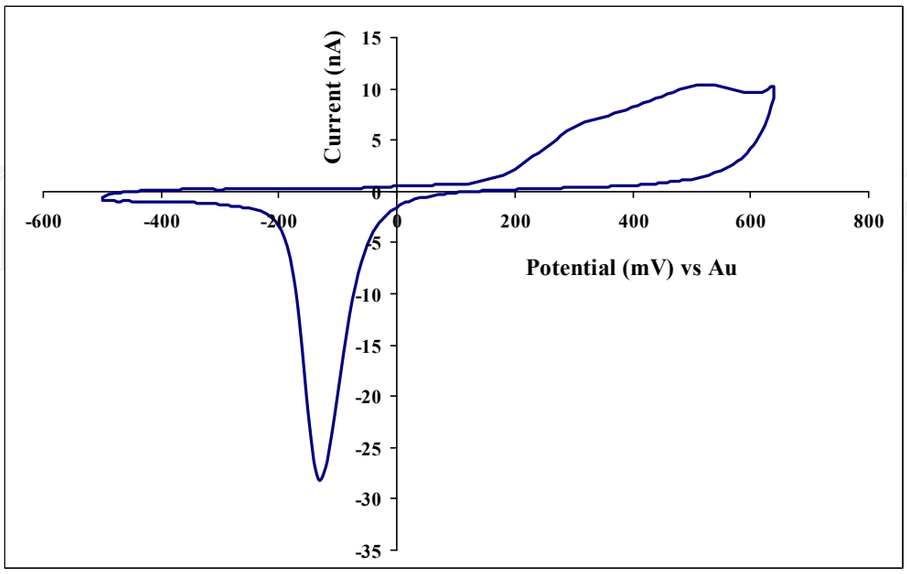


Fig. 5. Typical cyclic voltammogram of gold electrode obtained using 50 mM of $HClO_4$; scan rate: 100 mV/sec

1. The cleanness of the gold electrodes should be checked before performing the electroplating process. Cyclic voltammograms (CVs) in the range -500 - 700 mV and scan rate of 100 mV/cm using an ionic solution (e.g. 50 mM $HClO_4$) is performed. Figure 5 shows typical example of CV for clean gold surfaces, where observing the adsorption/desorption peaks of oxygen are efficient strategy for evaluating the cleanness of the gold electrodes surfaces.
2. Solution of K_2PdCl_6 (10 mM) is loaded into the waste reservoir (labeled as A in Figure 4) while applying vacuum to the waste reservoir (B) in order to fill the microchannel with the depositing solution.
3. Square potential signal is applied between 0 and -1800 mV from a potentiostat with a frequency of 2 Hz, see inset in Figure 4.

3.3.5 Electrophoresis

4. Prior to performing any electrophoresis separation process, the microchannels are flushed with a solution of NaOH (0.1 M) for 10 minutes followed by flushing with deionized water for another 10 min. The flushing is performed by loading the desired solution to the reservoirs a,b, and c while applying vacuum to the reservoir d.
5. After the flushing process, the microchannels are filled with the running buffer.
6. Fresh buffer and sample solutions are added loaded onto reservoirs a and b, respectively.
7. After the sample is injected (see below), a separation voltage is applied in the range 100-300 V/cm. For each separation process, fresh buffer solution is loaded.

3.3.6 Injection

Simplified gated injection is applied, where single power supply is used for injection and separation, via which a variable resistor is connected to the sample reservoir; hence, a relevant voltage is applied to the sample reservoir (e.g. 75% of that is applied to the buffer reservoir). Figure 6 illustrates detailed procedure with real images for the injection process.

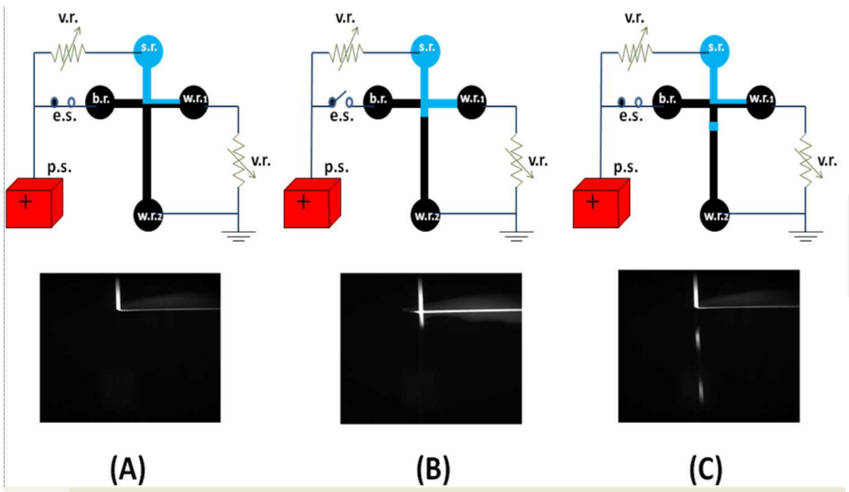


Fig. 6. Illustration of the simplified gated injection process using single power supply. Left column: schematic operation; right column: experimental imaging of real injection process. Frames A, B, and C correspond to the pre-injection, injection, and the post-injection (separation) steps, respectively. Microfluidic labels: buffer reservoir (a), sample reservoir (b), waste reservoirs (c, d), variable resistors (R1, R2); injection time: 1 sec.

The injection process consists of 3 steps:

1. Pre-injection, where voltage is applied between reservoirs "b.r.-w.r.1" and "s.r.-w.r.1"; during this step, the sample solution fills the microchannel that connects reservoirs s.r. and w.r.1 while the flow of the buffer solution between reservoirs b.r. and w.r.1 prevents the sample solution to flow toward the separation channel.

Injection, the electrode in b.r. is floated for approximately 1 sec, which causes the sample solution to flow toward the separation channel.

2. Post-injection (separation), the electrode in b.r. is reconnected, and hence the conditions for the pre-injection are resumed; however, a sample plug is generated and the separation process begins.

3.4 Electrochemical detection

All electrochemical measurements are performed using 3-electrode configuration with in-channel and end-channel detection; in both arrangements the auxiliary and reference electrodes are located inside the waste reservoir d:

3.4.1 End-Channel detection

The working electrode is located at very short distance from the separation channel exit (~ 15 μm) and inside the waste reservoir d. An array of ten microelectrodes that can serve as individual working electrodes is fabricated in order to assure locating the working electrode abruptly after the separation channel exit. The position of the working electrode is optimized using the microelectrodes array that spreads over a total distance of approximately 1 mm, which offers positioning the microelectrodes at different locations from the separation channel exit. Within this arrangement, the working electrode is located before the electrophoretic ground, and hence both electrodes are located inside the waste reservoir d.

3.4.2 In-Channel detection (implementing Pd decoupler)

The working electrode is located inside the separation channel e, after the electrophoretic ground. Within this arrangement, a decoupler is introduced via electrodepositing palladium particles on the surface of the first microelectrode of the array (electrode # 1 in Figure 3). The distance between the decoupler and the working electrode is optimized using the microelectrodes 2 to 10 individually.

After optimizing the location of the working electrode, optimizing the amperometric detection before the separation process is needed for each arrangement. The optimized detection potential for each analyte is determined through constructing the hydrodynamic voltammograms under similar injection and separation conditions. Figure 7 shows typical hydrodynamic voltammograms for various analytes of interests, including the 4DA-6-N7Gua and 8-OH-dG DNA adducts.

4. Discussion and technical notes

Various issues and technical approaches have to be considered upon performing analyses using the microfluidic MEMS. Among these issues, stability of the DNA adducts is critical issue, where leaving the sample solution at room temperature for a long time could lead to oxidizing the DNA adducts and their related analytes, especially at basic pH. Observing

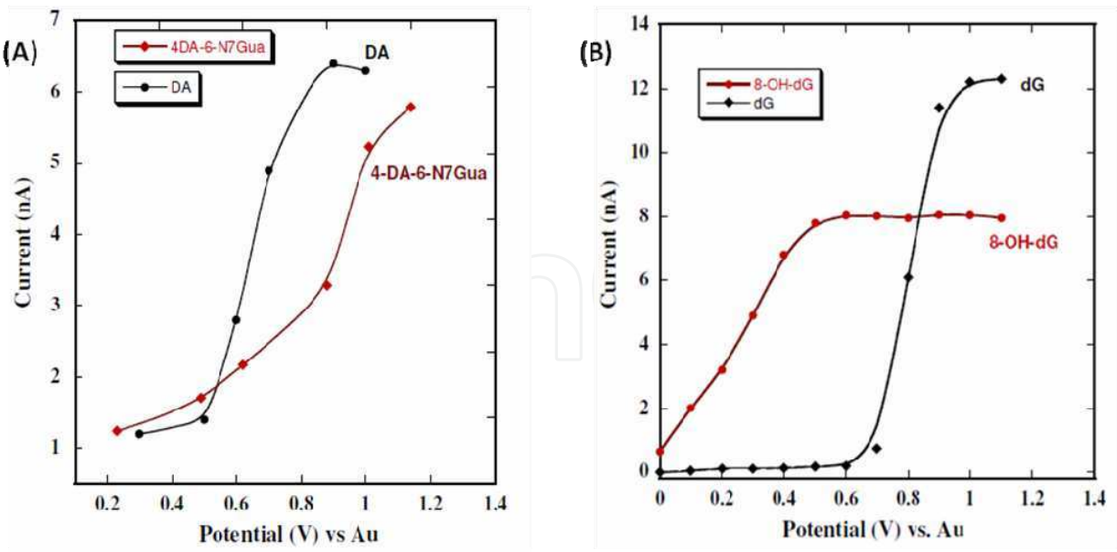


Fig. 7. Hydrodynamic voltammograms of DA (380 μM) and 4DA-6-N7Gua adduct (500 μM), and dG (50 μM) and 8-Oh-dG adduct (75 μM) obtained using end-channel and in-channel with electroplated Pd decoupler ECD, respectively. Operating conditions: 10 mM borate buffer at pH 9.1, injection time: 1 sec; separation electric field: 200 and 300 V/cm for A and B, respectively.

brownish color for the 4DA-6-N7Gua adduct and related neurotransmitters is indication for the formation of the corresponding quinones as a result of the oxidation reaction in solution. Hence, preserving the analytes solutions at low temperature (-20˚C) is essential for increasing the lifetime of the analytes under investigation.

The dimensions of the microchannels are controlled by the photomask and the photoresist viscosity; while the length and the width of the microchannels are controlled by the photomask dimensions, the viscosity of the photoresist controls the depth of the microchannels. Importantly, choosing the right photoresist with certain viscosity and following the recipes provided by the photoresist vendor are essential for obtaining the desired microchannels' depth. The microchannels' dimensions are critical for obtaining stable electrochemical signal. Hence, wide and shallow microchannels are recommended for obtaining stable detection current, where deep microchannels exhibit high electrophoretic current, which in turn reduces the stability of the background detection current. In addition, Starting with ultra clean microscopic glass slides is essential for obtaining good adhesion of the metals on the glass surface, which in turn can increase the durability of the microelectrodes. Furthermore, the titanium layer is needed to serve as seed layer for the gold layer. While other metals, such as chromium can be used too, titanium exhibits better adhesion properties toward the glass surface. Titanium layer > 10 nm is not recommended, where thicker layer of titanium requires using special etchant that may etch the upper layer of gold, and hence losing the continuity of the microelectrodes strips. Also, following the instruction that are provided by the photoresist (AZ-5214) vendor for processing the gold payer patterning is recommended for obtaining defined shapes for the gold microelectrodes stripes. The concentration of the gold etchant is critical in obtaining defined shapes for gold microelectrodes stripes, where more concentrated etchant needs shorter etching time. As the

iodine-based gold etchant has deep blue color, it is hard to observe the completion of the etching process, and hence checking out the etching process periodically is recommended. Etching for a long time could cause to break the continuity of the gold microelectrodes stripes.

Using different materials for fabrication the microelectrode that serve as working electrode can also be utilized [40,41]. In particular, carbon electrodes can exhibit lower noise current and wider detection window. Such features are of significant importance upon analyzing electrochemically chemical species with large geometrical structures, such as codeine and related metabolites. Figure 8 shows normalized CVs of four related materials of forensic interests, namely codeine, morphine, hydromorphone and normorphine. Interestingly, carbon ink based electrodes exhibit background CV that is comparable to CV observed for commercial glassy carbon electrodes frequently used electrochemical experimentation, which has characteristic importance in analyzing electrochemically chemical species at relatively high potential such as codeine.

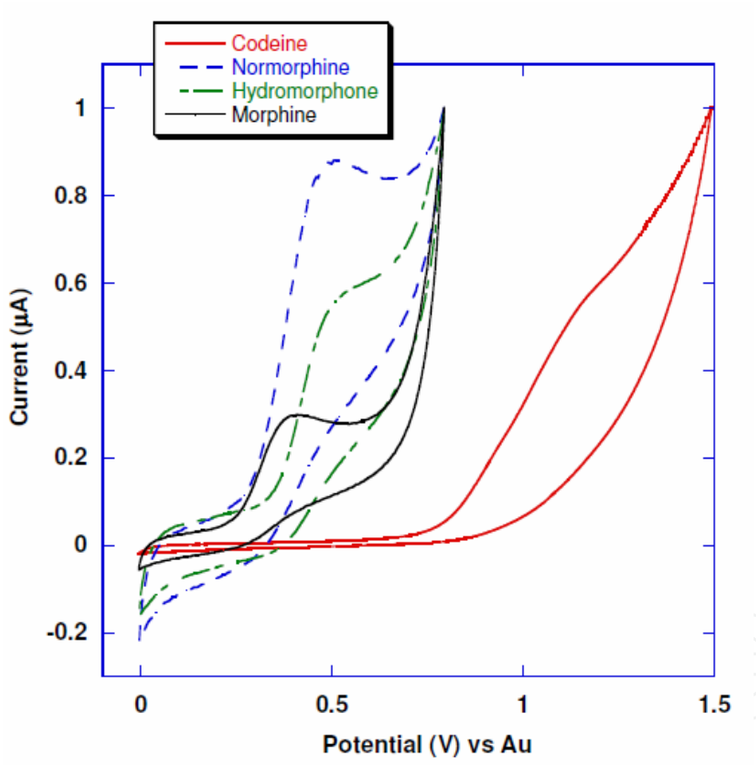


Fig. 8. Normalized CV of codeine, morphine, normorphine, and hydromorphone over CI electrode 10mM MES buffer. Scan rate 100 mV/s.

While the reversible binding of the PDMS slab to the gold-patterned glass substrate is easier to perform than the irreversible binding, microchannels with hydrophobic surfaces are produced, and hence difficulties in filling the microchannels are observed in addition to retarded electroosmotic flow. In addition, reversibly assembled microdevice cannot stand higher pressure that could be developed because of generating air bubbles, which in turn could damage the microdevice. On the other hand, irreversibly assembled microdevice can

stand much higher pressure with preferably hydrophilic microchannels. However, it is worth mentioning that the plasma-treated PDMS surfaces have to be assembled within approximately 3 min to obtain strong binding, where the PDMS surfaces notably lose their binding strength after exposing to air for longer time. Furthermore, the hydrophilic microchannels can retain their hydrophilicity for approximately 1 hr upon being exposed to air. Thus, it is highly recommended to keep the microchannels wet using aqueous solutions, e.g. filling the microchannels with the running buffer or water immediately after the assembling process. Interestingly, the array of the microelectrodes over a total distance of approximately 1 mm facilitates the process of the aligning process without using microscopes.

It is noteworthy mentioning that the cleanness of the microelectrodes surfaces is critical issue for obtaining high sensitivity and hence reliable analysis. As it is expected that the gold surface could get contaminated during the fabrication process, it is essential to ensure that the microelectrodes surfaces are ultra cleaned before performing any ECD. Also, clean surfaces are necessary for obtaining stable palladium electrophoretic ground produced using the electroplating technique. The length of the electroplating process strongly depends on the desired density of the palladium electroplated decoupler, which in turn depends on the applied separation electric field and the running buffer. For high density of electroplated palladium, longer deposition time is needed (e.g. 4 min); meanwhile, applying vacuum periodically during the electroplating process to the other end of the microchannel in order to refresh the electroplating solution is recommended for obtaining efficient electroplating process. It is noteworthy that vigorous formation of air bubbles at the electrophoretic ground may cause the electroplated palladium particles to be released from the gold surface, and hence interrupting the separation process.

Obtaining electrophoretic separation with high resolution depends on several factors including the separation channel length, the running buffer, and the applied separation electric field. As longer separation channel is expected to offer better resolution, longer analysis time is observed, which contradicts the advantageous features of using microfluidic devices to perform chromatographic and electrophoretic separation. On the other hand, performing the electrophoretic separation at low separation electric field could lead to diffusion-controlled detection process, and hence reduced sensitivity is observed. However, higher separation electric field has the advantages of observing better sensitivity due to more efficient interaction between the analyte and the electrochemical sensing electrode. Unfortunately, less stable and high level of background detection current is observed for end-channel detection current. However, reduced effect for the higher separation electric field is observed for the in-channel detection with palladium decoupler, and hence notable enhanced sensitivity and stability of the in-channel detection is observed. Figure 9 shows the effect of the applied separation voltage on the capillary electrophoretic separation of 8-OH-dG and dG. For ECD interfaced with capillary electrophoresis, the electrophoretic current strongly affects the detection current; thus, using running buffer with low ionic mobility is recommended. Hence, MES buffer is widely used as running buffer for ECD interfaced with CE. However, using MES buffer as the running buffer for performing an electrophoretic separation of a mixture of 4DA-6-N7Gua, dopamine, L-tyrosine, L-DOPA, and catechol, and a mixture of dG and 8-OH-dG generated electropherograms with only two and one peaks, respectively. Interestingly, although borate buffer exhibit higher ionic mobility than MES

buffer, significantly enhanced resolution is observed. Figure 10 shows an electropherogram for the separation of a mixture of 4DA-6-N7Gua, dopamine, L-tyrosine, L-DOPA, and catechol obtained using borate buffer with end-channel ECD arrangement. Generally, optimizing the separation process strongly depends on the nature of the analytes under investigation, where each separation parameter has to be optimized separately.

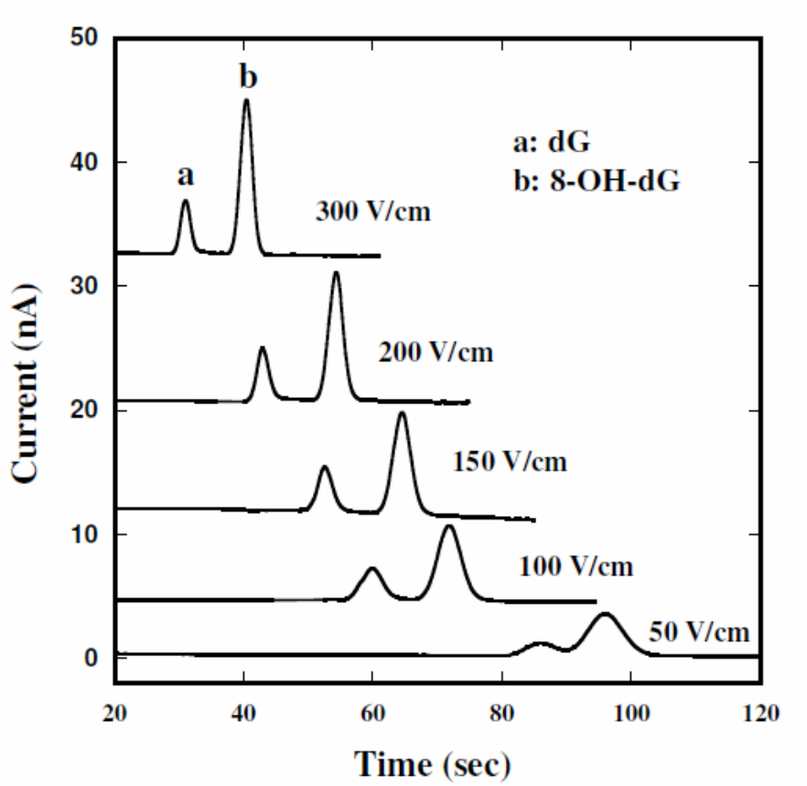


Fig. 9. Separation of dG (50 μM) and 8-OH-dG adduct (75 μM) at various separation electric fields. Operating conditions:10 mM borate buffer (pH 9.5), injection time: 1 sec, EC potential: 900 mV vs Au.

PDMS has weak heat dissipation capability, and hence high Joule's heating that is observed at high electrophoretic current could cause severe damage to the microfluidic device. As can be seen in Figure 3, the variable resister # 2 that is connected in series with waste reservoir (w.r. 1) provides comparable electric field along the injection microchannel to that is observed along the separation channel. Such arrangement is essential while using single power supply for injection and separation. Gated injection offers variable sample plug's size, where more intense signal is observed for long injection time (e.g. 2-5 sec). However, large sample plug's size generates low resolution. Hence, optimizing the injection time is performed depending on the complexity of the mixture to be analyzed, where shorter injection time is recommended for more complex sample. Finally, the durability of the microfluidic device depends mainly on the lifetime of the sensing electrodes. Working electrode passivation during the ECD, which results from the adsorption of some oxidized analytes, could reduce the sensitivity of the working electrode. Thus, applying sinusoidal wave potential regularly and after each injection process is recommended.

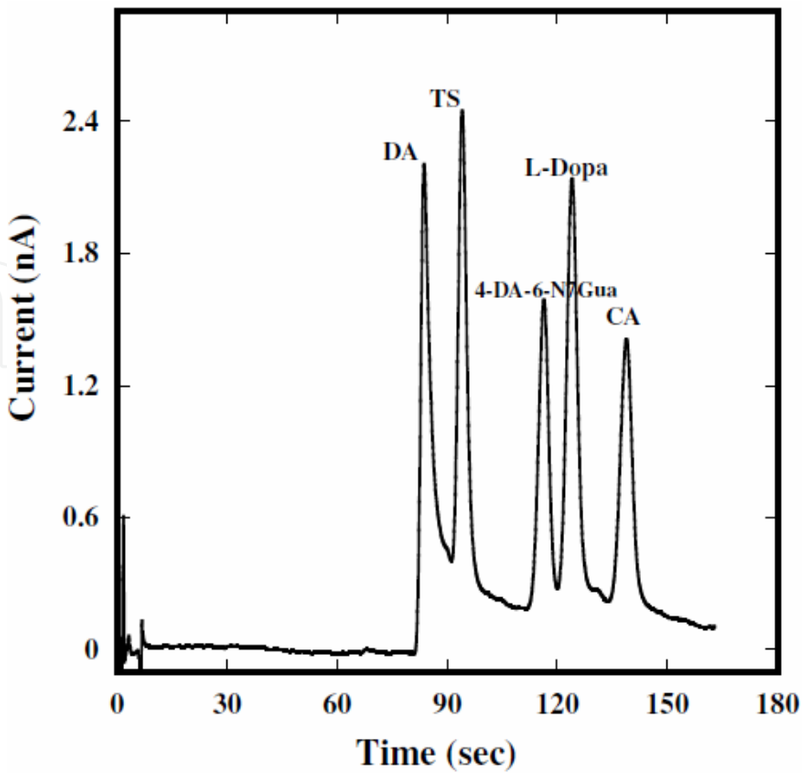


Fig. 10. Electropherogram for the separation of a mixture of 200 μM 4-DA-6-N7Gua adduct and related analytes. Operating conditions: 10 mM Borate buffer (pH 9.1), separation electric field: 140 V/cm, injection time: 1 sec, EC potential: +1000 mV vs Au.

5. Acknowledgement.

The author is grateful to the Strategic Research Unit at Taibah University (Nanotechnology Program Project Grant 08-NANO-22-05) for partial support of the work. The author also is thankful to Dr. Elham Mohammad at Taibah Universuty, Prof. R.Jankowiak at Kansas State University (KS, USA), and Dr. T. Kawaguchi at Hokaido University (Japan) for their valuable discussion and support.

6. Reference

[1] Manz, A., Grabner, N., Widmer, H.M. (1990) Miniaturized total chemical analysis systems: a novel concept for chemical sensing. *Sens. Actuators B* 1, 244–248.

[2] Harrison, D.J., Manz, A., Fan, Z., Lüdi, H., Widmer, H.M. (1992) Capillary electrophoresis and sample injection systems integrated on a planar glass chip. *Anal. Chem.* 64, 1926–1932.

[3] Lenshof A, Ahmad-Tajudin A, Jaras K, Sward-Nilsson AM, Aberg L , Marko-Varga G, Malm J, Lilja H (2009) Acoustic whole blood plasmapheresis chip for prostate specific antigen microarray diagnostics, Anal Chem 81 (15): 6030.

[4] Sollier E, Cubizolles M, Fouillet Y, Achard JLA (2010) Fast and continuous plasma extraction from whole human blood based on expanding cell-free layer devices, Biomed. Microdev 12 (3): 485.

[5] Munro NJ, Snow K, Kant JA, Landers JP (1999) Molecular diagnostics on microfabricated electrophoretic devices: from slab gelto capillary- to microchip-based assays for T- and B-cell lymphoproliferative disorders. Clin. Chem. 45: 1906.

[6] Kartalov EP, Lin DH, Lee DT, Anderson WF, Taylor CR, Scherer AA (2008) Internally calibrated quantification of protein analytes in human serum by fluorescence immunoassays in disposable elastomeric microfluidic devices, Electrophoresis 29 (24): 5010.

[7] Dawoud AA, Saryia H, Lazar IM (2007) Microfluidic platform with mass spectrometry detection for phosphoproteins analysis. Electrophoresis 28: 4645.

[8] House DL Chon CH, Creech CB ,Skaar EP, Li DQ (2010) Miniature on-chip detection of unpurified methicillin-resistant Staphylococcus aureus (MRSA) DNA using real-time PCR. J Biotechn 146: 93.

[9] Armenta JM, Dawoud AA, Lazar IM, Microfluidic chips for protein differential expression profiling. Electrophoresis 30: 1145.

[10] Lee, Park SH, Chung KH, Pyo HB (2008) A disposable plastic-silicon micro PCR chip using flexible printed circuit board protocols and its application to genomic DNA amplification. IEEE Sensors J 8 (6): 558.

[11] Ramalingam N, Rui Z, Liu HB, Dai CC, Kaushik R, Ratnaharika B, Gong HQ (2010) Real-time PCR-based microfluidic array chip for simultaneous detection of multiple waterborne pathogens Gong, Sens. Actuat. B Chem. 145: 543

[12] Sung JH, Kam C, Shuler ML (2010) A microfluidic device for a pharmacokinetic-pharmacodynamic (PK-PD) model on a chip. Lab Chip 10 (4): 446.

[13] Wen Y, Yang ST (2008) The future of microfluidic assays in drug development. Expert Opin Drug Discov 3: 1323

[14] Li X, Huang J, Tibbits GF, Li PCH (2007) Real-time monitoring of intracellular calcium dynamic mobilization of a single cardiomyocyte in a microfluidic chip pertaining to drug discovery, Electrophoresis 28 (24) 4723.

[15] Shen SL, Li Y, Wakida SA (2010) Characterization of dissolved organic carbon at low levels in environmental waters by microfluidic-chip-based capillary gel electrophoresis with a laser-induced fluorescence detector. Environ. Monit Assess 166: 573.

[16] Chen G, Lin Y, Wang J (2006) Monitoring environmental pollutants by microchip capillary electrophoresis with electrochemical detection. Talanta 68: 497.

[17] Wakida S, Fujimoto K, Nagai H, Miyado T, Shibutani Y, Takeda S (2006) On-chip micellar electrokinetic chromatographic separation of phenolic chemicals in waters. J Chromatogr A 1109: 179.

[18] Masadome T, Nakamura K, Iijima D, Horiuchi O, Tossanaitada B, Wakida S, Imato T (2010) Microfluidic polymer chip with an embedded ion-selective electrode detector for nitrate-ion assay in environmental samples Anal Sciences 26: 417.

[19] Woolley, A.T., Mathies, R.A. (1995) Ultra-high-speed DNA sequencing using capillary electrophoresis chips. *Anal. Chem.* 67, 3676–3680.

[20] Burns, M.A., Johnson, B.N., Brahmasandra, S.N., Handique, K., Burke, D.T. (1998) An integrated nanoliter DNA analysis device. *Science* 282, 484–487.

[21] Dolník, V., Liu, S., Vladisl, S.J. (2000) Capillary electrophoresis on microchip. *Electrophoresis* 21, 41–54.

[22] Woolley, A.T., Lao, K., Glazer, A.N., Mathies, R.A. (1998) Capillary electrophoresis chips with integrated electrochemical detection, *Anal. Chem.* 70, 684–688.

[23] Chabinyc, M.L. (2001) An integrated fluorescence detection system in poly (dimethylsiloxane) for microfluidic applications, *Anal. Chem.* 73, 4491–4498.

[24] Malic, L., Kirk, A.G. (2007) Integrated miniaturized optical detection platform for fluorescence and absorption spectroscopy. *Sens. Actuators A* 135, 515-524.

[25] Ro, K.W., Lim, K., Shim, B.C., Hahn, J.H. (2005) Integrated light collimating system for extended optical-path-length absorbance detection in microchip-based capillary electrophoresis. *Anal. Chem.* 77, 5160-5166.

[26] Dawoud, A.A., Kawaguchi, T., Markushin, Y., Porter, M.D., Jankowiak, R. (2006) Separation of catecholamines and dopamine-derived DNA adduct using a microfluidic device with electrochemical detection. *Sens. Actuators B* 120, 42–50

[27] Dawoud, A.A., Kawaguchi, T., Jankowiak, R. (2007) Integrated microfluidic device with an electroplated palladium decoupler for more sensitive amperometric detection of the 8-hydroxy-deoxyguanosine (8-OH-dG) DNA adduct. *Anal. Bioanal. Chem.* 388, 245-252.

[28] Dawoud, A.A., Kawaguchi, T., Jankowiak, R. (2007) In-channel modification of electrochemical detector for the detection of bio-targets on microchip. *Electrochem. Comm.* 9, 1536–1541

[29] Singh, R., Todorovic, R., Devanesan, P., Higginbotham, S., Zhao, J., Gross, M.L., Rogan, E.G., Cavalieri, E.L. (2001) Analysis of potential biomarkers of estrogeninitiated cancer in the urine of Syrian golden hamsters treated with 4-hydroxyestradiol. *Carcinogenesis* 22, 905–911.

[30] Shigenaga, M., Gimeno, C., Ames, B. (1989) Urinary 8-hydroxy-2'-deoxyguanosine as a biological marker of in vivo oxidative DNA damage, *Proc. Natl. Acad. Sci.* 86, 9697-9701.

[31] Hemminki, K. (1983) Nucleic acid adducts of chemical carcinogens and mutagens. *Arch. Toxiocol.* 52, 249-285.

[32] Dipple, A. (1995) DNA adducts of chemical carcinogens. *Carcinogenesis* 16, 437-441.

[33] Wogan, G.N., Hecht, S.S., Felton, J.S., Conney, A.H., Loeb, L.A. (2004) Environmental and chemical carcinogenesis. *Semin. Cancer Biol.* 14, 473-486.

[34] Luch, A. (2005) Nature and nurture lessons from chemical carcinogenesis. *Nat. Rev. Cancer* 5, 113-125.

[35] Markushin, Y., Gaikwad, N., Zhang, H., Kapke, P., Rogan, E.G., Cavalieri, E.L., Trock, B.J., Pavlovich, C., Jankowiak, R (2006) Potential biomarker for early risk assessment of prostate cancer. *Prostate* 66, 1565–1571.

[36] Markushin, Y., Kapke, P., Saeed, M., Zhang, H., Dawoud, A.A., Rogan, E., Cavalieri, E.G., Jankowiak, R. (2005) Development of monoclonal antibodies to 4-hydroxyestrogen-2-N-acetylcysteine conjugates: immunoaffinity and spectroscopic studies. *Chem. Res. Toxicol.* 18, 1520-1527.

[37] Hunter, R.J., *Zeta Potential in Colloid Science: Principles and Applications*, Academic Press, (1981), pp 1-56.

[38] Delgado, A. V., *Interfacial Electrokinetics and Electrophoresis*, Marcel Dekker, New York (2002), pp 1-54.

[39] Cavalieri, E.L., Li, K.-M., Balu, N., Saeed, M., Devanesan, P., Higginbotham, S., Zhao, J., Gross, M.L., Rogan, E.J. (2002), Catechol ortho-quinones: the electrophilic compounds that form depurinating DNA adducts and could initiate cancer and other diseases. *Carcinogenesis* 23, 1071– 1077.

[40] Dawoud Bani-Yaseen, A.A. (2009), Fabrication and Characterization Fabrication of Fully Integrated Microfluidic Device with Carbon Sensing Electrode for the Analysis of Selected Biomedical Targets. IEEE Sensors J. 9 (2), 81-86.

[41] Dawoud Bani-Yaseen, A.A., Kawaguchi, T., Jankowiak, R. (2009), Electrochemically Deposited Metal Nanoparticles for Enhancing the Performance of Microfluidic MEMS in Biochemical Analysis. Int. J. Nanomanufact., 4, 99-107.

IntechOpen



Biomedical Engineering, Trends in Electronics, Communications and Software

Edited by Mr Anthony Laskovski

ISBN 978-953-307-475-7
Hard cover, 736 pages
Publisher InTech
Published online 08, January, 2011
Published in print edition January, 2011

Rapid technological developments in the last century have brought the field of biomedical engineering into a totally new realm. Breakthroughs in materials science, imaging, electronics and, more recently, the information age have improved our understanding of the human body. As a result, the field of biomedical engineering is thriving, with innovations that aim to improve the quality and reduce the cost of medical care. This book is the first in a series of three that will present recent trends in biomedical engineering, with a particular focus on applications in electronics and communications. More specifically: wireless monitoring, sensors, medical imaging and the management of medical information are covered, among other subjects.

How to reference

In order to correctly reference this scholarly work, feel free to copy and paste the following:

Abdulilah A. Dawoud Bani-Yaseen (2011). Integrated Microfluidic MEMS and Their Biomedical Applications, Biomedical Engineering, Trends in Electronics, Communications and Software, Mr Anthony Laskovski (Ed.), ISBN: 978-953-307-475-7, InTech, Available from: http://www.intechopen.com/books/biomedical-engineering-trends-in-electronics-communications-and-software/integrated-microfluidic-mems-and-their-biomedical-applications

INTECH
open science | open minds

InTech Europe
University Campus STeP Ri
Slavka Krautzeka 83/A
51000 Rijeka, Croatia
Phone: +385 (51) 770 447
Fax: +385 (51) 686 166
www.intechopen.com

InTech China
Unit 405, Office Block, Hotel Equatorial Shanghai
No.65, Yan An Road (West), Shanghai, 200040, China
中国上海市延安西路65号上海国际贵都大饭店办公楼405单元
Phone: +86-21-62489820
Fax: +86-21-62489821

© 2011 The Author(s). Licensee IntechOpen. This chapter is distributed under the terms of the Creative Commons Attribution-NonCommercial-ShareAlike-3.0 License, which permits use, distribution and reproduction for non-commercial purposes, provided the original is properly cited and derivative works building on this content are distributed under the same license.

IntechOpen

IntechOpen